[Frontiers in Bioscience 7, d1195-1211, May 1, 2002]

CA^{2+} RELEASE FLUX UNDERLYING CA^{2+} TRANSIENTS AND CA^{2+} SPARKS IN SKELETAL MUSCLE

Eduardo Ríos [1] and Gustavo Brum [2]

[1] Department of Molecular Biophysics and Physiology, Rush University, 1750 W. Harrison Street, Chicago, IL 60612,
[2] Departamento de Biofísica, Facultad de Medicina, Universidad de la República, G. Flores 2125, Montevideo, Uruguay

TABLE OF CONTENTS

1. ABSTRACT

Three main paths to derive the Ca^{2+} release flux underlying Ca^{2+} sparks are reviewed here: Some properties of release flux can be inferred from an examination of spark morphology. Others from model simulations, which generate sparks assuming an ion source within a cytoplasm-like medium. Finally, the release flux can be derived from the fluorescence transient by generalizing an algorithm developed earlier for global or whole cell signals. The transient and spatially limited nature of sparks adds many uncertainties to the process. These methods yield estimates between 1.4 and 30 pA, not clearly greater in skeletal than in cardiac muscle. At their low end, the estimates are consistent with generation of sparks by one or two ryanodine receptor channels, but the results are easier to explain if several channels, from as little as four to as many as 60, cooperate in their generation. How release flux determines spark shape and time course has been understood largely through simulations. The rise time of sparks corresponds to active release time. Both release flux and release time may vary among individual sparks, leading to their varied size and shape. Release flux turns off abruptly, therefore the decay of sparks is determined by Ca^{2+} removal and diffusion. Spatial width increases with release time (rise time). That its experimentally determined value is too large compared with simulations, remains the single most important question in the interpretation of shape. Sparks are not the sole form of local fluorescence transients. When channel opening drugs are present, or sometimes spontaneously, sparks may be prolonged by embers. If the release flux calculated during an ember corresponds to a single open channel, then the release underlying a spark must require many open channels. The continued examination of Ca^{2+} release flux appears to be an essential requisite for the interpretation of sparks and their place in calcium signaling.

2. INTRODUCTION

Ca^{2+} sparks (1) are regarded as Athe elementary events@ of Ca^{2+} release in skeletal and cardiac muscle. This

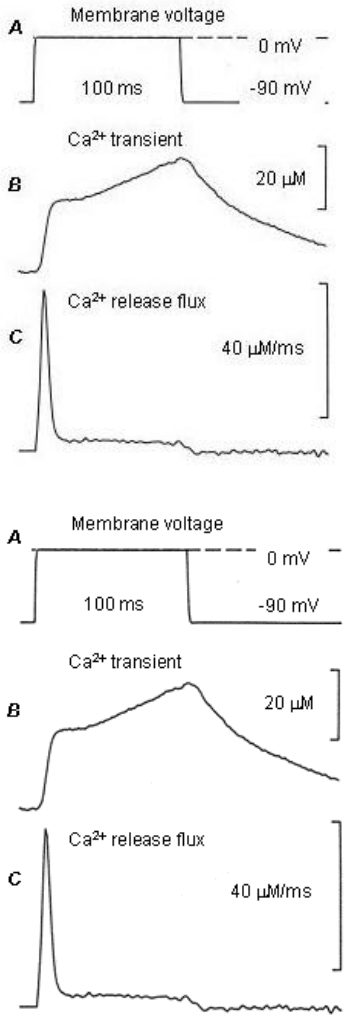

Figure 1. The analysis of global signals. The pulse at top was applied to a frog fiber under voltage clamp. The Ca^{2+} transient was derived from the absorption change of the dye ApIII according to eqn. 1. The release flux record was derived from the Ca^{2+} transient using text eqn. 2. Removal flux was derived applying the method of Melzer et al. (3,4) to the Ca^{2+} transient shown and other transients not shown. Modified from Ríos and Pizarro (5).

concept has four components. One is semantic: Ca^{2+} sparks are really fluorescence events, reflecting a transient increase in the concentration of a Ca^{2+}-bound dye. Hence they are primarily related to and driven by an increase in $[Ca^{2+}]_i$. In that sense they are the local equivalent -- the elementary unit-- of the ACa^{2+} transient@ that takes place in the whole cell. Therefore, a more punctilious enunciation of the first concept is that *the Ca^{2+} release underlying a spark constitutes the elementary unit of cellular Ca^{2+} release*. A main topic of this article is how to derive from the (fluorescence) spark the underlying Ca^{2+} release.

The second element in the idea of Aelementary event@ is that they enter the whole additively, superimposed, much as bricks pile up in a wall. While there are some evidences that such is the case, there are ways other than addition to compose whole cell release. Say that sparks are generated by single channels or pairs of channels gating in unison. Then assume that one channel, or one pair, can gate another (channel or pair) if both are close to each other. This would imply that the spark generators interact, no longer constituting real units of release generation. In other words, the mathematics would in this case become more complex than addition, and the concept of sparks as units would lose much validity.

Another ingredient of the Aelementary event@ concept is that it is indivisible, atomic. Of course, this would be a property of sparks produced by single openings of single channels. Whether or not this is the case constitutes one of the main questions posed by the existence of sparks, and the answer has powerful consequences for mechanism. Any discussion of flux under a spark is basically an argument about composition of the spark generator Bwhether it is composed of many channels, or a single one.

Our opening statement contains yet a fourth idea, that sparks constitute the sole components of whole cell release. The question is whether in addition to bricks there is some sand or gravel in the release construction.

The above considerations should stress that sparks are studied to understand a cellular process, Ca^{2+} release, and its control. It should also be a reminder that our only experimental approach to these processes is to measure a transient in the concentration of the Ca^{2+}-bound form of a fluorescent dye. Everything else: the Ca^{2+} transient, the release flux, and its mechanisms, are inferred from that single measurement.

3. FROM GLOBAL CA^{2+} SIGNAL TO CA^{2+} RELEASE FLUX.

Current calculations of release under Ca^{2+} sparks draw heavily from earlier work on whole cell Ca^{2+} transients. Consequently, before examining the issue at the spark (or local) level, it is instructive to consider the question of release flux at the macroscopic or global level.

The measurement of global Ca^{2+} transients may be carried out using any fluorescent Ca^{2+} indicator (though it was initially done with absorption dyes, mainly the fast-equilibrating Antipyrylazo III). In cells stimulated by action potential or voltage clamp, the signal $S(t)$ (an absorption or a fluorescence) is a linear function of the bound dye, its change over time trailing the Ca^{2+} transient by an interval determined by the kinetic constants of the dye-Ca^{2+} reaction, most importantly the off rate constant, k^-. The derivation of $[Ca^{2+}](t)$ from S involves solving a first order differential equation (see for instance ref. 2), the solution of which has the following form:

$$[Ca^+](t) = \frac{\frac{dS}{dt} + k^-(S - S_{min})}{k^+(S_{max} - S)} \qquad (1)$$

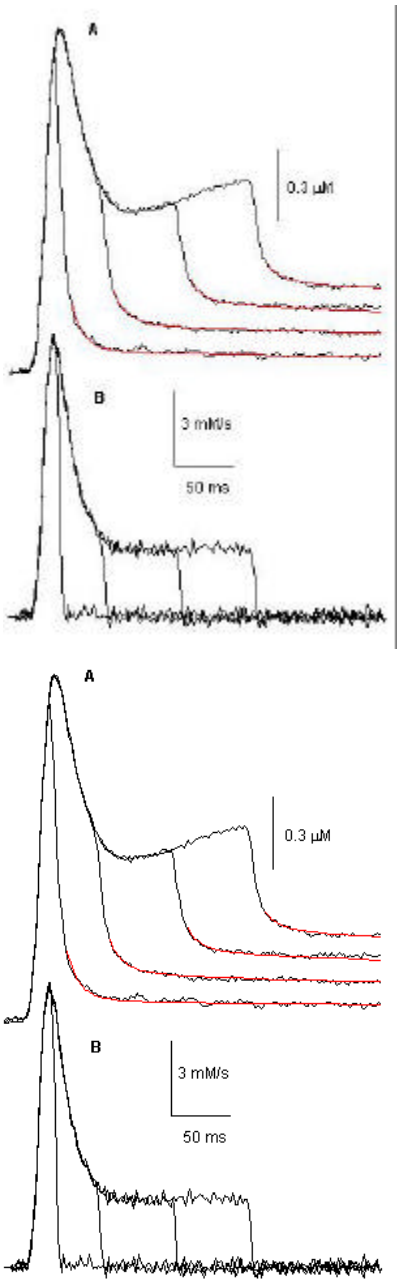

Figure 2. Ca^{2+} transients and flux in the presence of a slow buffer. A, Ca^{2+} transients (measured in a frog fiber, using antipyrylazo III) obtained in response to pulses of various durations to -40 mV. Lines in red represent Ä[Ca^{2+}](t) predicted by the removal model during determination of release flux. B, the corresponding release flux records. Note how the presence of EGTA in the internal solution (12 mM) modified the Ca^{2+} transients (compared with those of fig. 1) bringing their time course closer to that of the release flux. From Shirokova *et al.* (2), modified.

Note the presence of a term proportional to the derivative of the signal (the weight of which decreases if k^- is high). This differentiation step increases the weight of the high frequency component in the signal. Thus the high frequency terms of the noise (which tends to have a flat spectrum) become more significant.

The next step is to derive the flux of Ca^{2+} release from the Ca^{2+} transient. This question was solved in two different ways (3, 4, 6). A Ca^{2+} transient elicited by a voltage pulse, and the calculated release flux (3,4) are in Figure 1. Both approaches are based on an equation for release flux, $R(t)$,

$$R = d[Ca^{2+}]/dt + drem/dt \quad (2)$$

whereby release flux is equated to the sum of the rate of change of free $[Ca^{2+}]_i$ plus a rate of Ca^{2+} removal by binding sites and other processes. Baylor *et al.* (6) calculated the *net flux of Ca^{2+} exiting the SR* as the sum of the rate of change of $[Ca^{2+}]_i$ (t) plus the rate of binding of Ca^{2+} to the known cytoplasmic binding sites. The latter was calculated as the binding flux driven by the measured $[Ca^{2+}]_i$ (t), using literature values of ligand concentrations and their kinetic constants. Instead of using $[Ca^{2+}]_i$ (t) to drive reactions with assumed kinetics, Melzer *et al.* (3,4) fitted (concentrations and binding constants of) a removal model, so that its $[Ca^{2+}]_i$ would evolve in the same way as the measured one when the flux stopped after the pulse (curves in red in Figure 2A)[1].

In both cases, the contribution by the removal terms was much more important than the rate of change of the free $[Ca^{2+}]_i$ **B** as most calcium in the cytoplasm is bound. For both methods, the calculation involved differentiation of $[Ca^{2+}]_i$ (t), so that second derivatives of the measured signal entered the final flux. The drawbacks of the calculation therefore included a sharp enhancement of noise in the measurement, and the uncertainties involved in assignment of values to the removal model, which as stated makes a crucial contribution to the total flux. The increase in noise may be offset by low-pass filtering, at the cost of blunting the prominent peak present in the Ca^{2+} release waveforms (figs 1 and 2B). These drawbacks would only become worse when these procedures were generalized to Ca^{2+} sparks.

Ways were concocted to improve the determination, which removed the uncertainty regarding the sequestering molecules by adding one to great excess over the others. For example, it was shown that a large concentration of the slow, high affinity chelator EGTA would not only eliminate much of the uncertainty regarding removal parameters (simply because EGTA would reduce $[Ca^{2+}]_i$ making the other components of removal less relevant) but also render the temporal waveform $[Ca^{2+}]_i$ (t) similar to that of release flux (7, 8, 9). This is illustrated in Figure 2, showing Ca^{2+} transients elicited in a frog fiber by pulses of various durations to the same low voltage (A). In contrast with fig.1, and due to the inclusion of 10 mM EGTA in the internal solution, the transients in this case have many of the kinetic properties of the release waveforms, plotted in B. On the other extreme, a *fast* Ca^{2+} buffer, like arsenazo III (10), antipyrylazo III or furaptra, at high concentrations, also reduces the magnitude of the

Table 1. Morphology of Ca^{2+} sparks

	Preparation	Amplitude	FWHM µm	FDHM Ms	Rise time ms	Reference
Frog skeletal	Voltage clamp	2.93	1.46	10.4	4.56	13
	Permeabilized	1.92	1.31	11.0	5.6	14
	Notched fibers	0.75	1.7	10	5.5	15
	Intact fibers	3.7-4.6	0.97-1.02	5.5-6.2	3.7- 4.6 *	16
Mammalian skeletal	Rat permeabilized	0.42	1.95	84	11.2	26
	Rat and mouse permeabilized skinned	1.80	2.0	48.1 15.1 †	49.3 17.5 †	17
	Devel. mouse myotubes voltage clamp	1.27	1.4	25.3		18
	RyR3 knockout mouse voltage clamp	1.30	1.63	43.6		18
Ventricular Myocytes	Rat intact cells	1.55	-	12.8‡	9.5	19
	Rat intact cells	1.85	1.98	23.7‡	-	58
	Rat cells: intact	1.67	1.75	27.7		20
	permeabilized	1.72	1.85	26.1		
	Rat intact cells	2.0	1.7-2.2	20§	-	21
	Mouse voltage clamp	1.65	-	23.7§	-	22
	Rat trabecula intact cells	1.9-2.8	-	40	5	23

* measured from 0-100 % amplitude, † mechanically skinned, ‡ half time of decay, § τ_{decay}.

change in $[Ca^{2+}]_i$, but alters its course to bring it close to the time integral of the release flux. Of course these added buffers, which change the Ca^{2+} transient directly, might alter Ca^{2+} release if Ca^{2+} affected gating of the release channels. It is remarkable, however, that the waveform of release flux during a voltage clamp pulse (Figure 1) is only slightly altered by EGTA at 20 mM (11, 8, 9).

The flux of Ca^{2+} release thus calculated, reaches maxima of about 180 mM/s during a large voltage clamp pulse in frog muscle, and in one action potential adds up to 0.5 mM, or 15% of the total releasable SR calcium (9, 2, 12).

4. Ca^{2+} SPARKS

Using conventional confocal microscopy, sparks can be observed either in *x-y* scans or in line scans. Release flux with reasonable temporal resolution can only be derived from line scans. A new difficulty, not confronted at the whole cell level, is that Aobject space@, where sparks reside as local fluorescent packets of high [dye:Ca^{2+}], must be translated to image space by the imaging system (microscope). That operation has two consequences: the image is rendered 2-dimensional (one dimensional in the case of line scans), and is also blurred in the *x-y* plane, becoming wider and flatter than the corresponding object. Hence the quantitative representation of spark morphology must be preceded by a correction, or deblurring. Because blurring is mathematically a convolution (an average or integral weighted by the PSF of the microscope), its correction consists of a deconvolution, which selectively enhances the weight of high spatial frequency components. This operation therefore increases noise of high spatial frequency, while the next step, derivation of the local Ca^{2+} transient, adds noise in both space and time.

After reconstruction of the Ca^{2+} transient, the process follows similar steps as the derivation of release flux from whole cell signals, and is described in section 5. Before attempting such calculation, however, we will simply describe Ca^{2+} sparks as functions of time and space. The events= size and shape should be clues to the underlying release flux.

4.1. Morphology of Ca^{2+} sparks

The Amorphometric@ parameters usually defined include amplitude (strictly, peak amplitude), spatial width, duration and rise time. Additionally, a better indication of size is given by the spark=s signal mass. Some published parameter values are collected in Table 1.

4.1.1. Amplitude

Measured spark amplitude varies widely from the lower limits of detection, (defined by noise, usually around 0.3 units of F_0) to high values of 14 in skeletal muscle (18) or 9 in ventricular myocytes (25). Fig 3 shows examples of sparks of high amplitude under two experimental conditions: (A) cut skeletal muscle fiber under voltage clamp, (B) a fiber permeabilized by saponin.

Amplitudes are usually much lower in permeabilized fibers (table 1). The reason may be quite simple: $\Delta F/F_0$ is approximately proportional to the relative increase in local $[Ca^{2+}]$. In the voltage clamp experiments the cell may be able to maintain a $[Ca^{2+}]_i$ substantially lower than in the solution at the cut ends, while in permeabilized fiber segments the free $[Ca^{2+}]$ will equilibrate rapidly within the cell at the solution value of 100 nM. The relative increase in $[Ca^{2+}]$ may therefore be lower in the latter case, simply because the initial value is higher (18).

Recently, we have been able to study a large number of sparks in adult rat EDL muscle (permeabilized by saponin). The amplitude of 2900 events was approximately 35% less than in frog fibers similarly prepared (26).

The distribution of spark amplitudes has been the subject of much scrutiny. Obviously, amplitude was taken as an indication of the magnitude of the underlying release, and the fact that several groups initially reported a modal distribution appeared to be consistent with the idea that sparks were generated by single channels. These observations were in error, as we now know. Indeed, all spark parameters, but most notably amplitude, are affected by a Afocusing@ error, due to the variable distance between the scanned line and the actual position of the source originating the spark. This error not only reduces the amplitude of detected sparks, but crucially alters the distribution of amplitudes, forcing it to be monotonous, without a mode (27, 28).

Izu *et al.* (29) and Cheng *et al.* (28) found that the distribution density of detected amplitudes of Gaussian sparks of constant size is inversely proportional to amplitude. Ríos *et al.* (30) used the result to devise a method of correction of the focusing error, which produced a Atrue distribution@ of amplitudes that had a large spread. In other words, sparks as *objects* have widely variable amplitudes. Additionally, in many cases a mode was present in the corrected distribution. The mode was more marked in the presence of caffeine, a well known promoter of the activation of release channels by Ca^{2+}. To interpret this result it must first be understood that a mode in spark amplitude does not necessarily imply a mode in Ca^{2+} release flux. It could, instead, correspond to a mode in the distribution of open times of the source. The implications of these alternatives will be clarified in section 5.1.

4.1.2. Spatial width

It is usually represented by the FWHM (full width at half magnitude) at the time of peak signal. In voltage-clamped frog cut skeletal muscle fibers in Cs glutamate-based internal solutions, the average value over events elicited by mild depolarization was 1.11 ìm (14). The value was greater (about 1.5 ìm) in fibers permeabilized with saponin or with notches (table 1). By contrast, in *intact* frog fibers the half width value (for spontaneous sparks, or those induced by increase in $[K^+]$), was close to 1 ìm (16). For mammalian Ca^{2+} sparks the width was approximately 20 % greater than in the similarly prepared frog muscles (26). In cardiac muscle, the values cover a range higher than that in skeletal muscle (table 1).

Width could be changed under some conditions: caffeine (1 mM) increased it in voltage-elicited sparks to 1.42 ìm (14; a smaller change in the same direction was reported in intact fibers, ref. 16). While reduction in $[Mg^{2+}]$ did not change width of sparks detected by Lacampagne *et al.* (32), increase in $[Mg^{2+}]$ to 7 mM (from a reference value of 0.6 mM) reduced the width of voltage-elicited sparks to 0.84 ìm (14). The implications of these numbers will be considered in section 5, by contrasting them with simulations of sparks.

4.1.3. Rise time

Defined as the interval between 10% and either 90% or 100% of the initial rise, it appears to be the parameter least sensitive to the focusing error (21, 33). Its average in frog cut fibers is about 4.8 ms (14, 15, 32) and in intact fibers about 4 ms (16). In mammalian skeletal muscle, the rise time was approximately 20% greater than in the comparable group of amphibian cells (26). Both rise time and duration of sparks appear to be longer in cardiac myocytes.

González *et al.* (14) and Lacampagne *et al.* (15) found no correlation among spark parameters, other than a week positive correlation between rise time and width (14). This correlation is present in most simulations of sparks (see below). It may explain why the spatial width of sparks in both cardiac myocytes and mammalian skeletal muscle is increased relative to the amphibian counterpart Bthei r rise times are also greater. It might also explain the widening effect of caffeine. However, when spatial widths were compared for groups of sparks of equal rise time in caffeine and reference, a significant difference was still found. Hence spark-widening by caffeine is a primary effect, which cannot be explained as consequential to a prolongation of rise time.

4.1.4. Signal mass

It is a function defined in line scans for every point in time, as the integral of the signal intensity over three-dimensional space (34). The determination of signal mass is difficult because volume integration multiplies the intensity by the square of the distance to the spark center, implying a large amplification of noise at long distances. For this reason, Shirokova *et al.* (18) suggested that it be approximated as the product of the amplitude by the volume of a sphere with diameter equal to FWHM. Although this turns out to be an underestimate[2], the valid concept is that signal mass will be proportional to the third power of any measure of spatial width. This is important because signal mass is related more closely to release flux than any other parameter, which suggests that the release flux underlying a spark should also depend on the third power of spatial width.

5. APPROACHES TO RELEASE FLUX

Researchers have used two methods to advance from simple description of spark morphology to the underlying release flux. In a constructive, inductive, or *forward* calculation, sparks Bi.e. the fluorescence image associated to the local distribution of dye:Ca^{2+}B were generated in simulations that started with a source of given current in a medium of set properties (27, 21, 13, 33, 25). The converse, deductive, or *backward* calculation was also attempted: to start from the measured dye:Ca^{2+} (in this case a function of t and spatial coordinates x), then derive the corresponding $[Ca^{2+}]_i$ (x, t) and deduce the release flux (35, 36, 13), much in the way it had been done earlier from the global Ca^{2+} transients.

5.1. Simulations

The first effort in this direction was carried out by Pratusevich and Balke (27). Theirs and all other models of individual sparks assume release to be a simple function of time, usually a pulse, originating at a point or a small (sub-resolution) sphere. The medium on which released

Ca^{2+} impinges is geometrically elaborate in the case of Pratusevich and Balke and later simulations of Jiang *et al.* (33), as they try to reproduce the structural layout of fixed binding and removal sites. Other simulations, instead, assume an aqueous medium with uniform properties, with binding sites that may be fixed, but are always at homogeneous density.

In the simulations of Pratusevich and Balke (27), assuming that release current was 1.4 pA, the sparks originating exactly in focus had an amplitude of 1.7. In the more detailed simulations of Jiang *et al.* (33), with parameters specifically copying skeletal muscle, the spark derived from a 1.4 pA source, open for 8 ms, had amplitude 1.1 and half width 1 ìm.

Assuming a homogeneous cytoplasm, Smith *et al.* (21) obtained sparks of up to 3.5 F_0 for a source of 2 pA. Again, the simulated sparks were much narrower than most experimental ones (FWHM ~ 1 ìm), and could only be widened, albeit slightly, by either eliminating the buffers, or spreading the source to a 0.6 ìm diameter. This study also noted a proportionality between peak amplitude of the signal and source current, a somewhat paradoxical observation given the fact that local [Ca^{2+}] reached values much greater than the K_D of the indicator (fluo-3). While this convenient result was explained as a consequence of the lack of equilibrium between dye and Ca^{2+} at short distances from the source (basically driving an irreversible transport of Ca^{2+} away from the source, on the dye), there was also a bad consequence, that the spatial properties of the Ca^{2+} transient were very poorly monitored. In other words, the lag with which the dye:Ca^{2+} signal follows the global Ca^{2+} transient is worsened in the case of the spatially resolved images, which both lag temporally and spatially dampen the Ca^{2+} transient.

The overall impression gathered from the simulations of Pratusevich and Balke (27), Smith et al., (21) and Jiang et al. (33), is that the sparks simulated for sources of intensity comparable to that of single RyRs in bilayers, have brightness (amplitude) and time course similar to those measured experimentally. These simulated sparks, however, have consistently a 0.8 to 1 ìm spatial width, while those measured experimentally range between 1.0 and 3 ìm. The large width of experimental sparks suggests that the release flux corresponds to much more than the 1 or 2 pA assumed in the simulations. Release flux should account, at the very least, for the signal mass, which is proportional to the total amount of Ca^{2+}:dye present. With other parameters equal, sparks differing by a factor of 2 in spatial width will differ in signal mass by a factor of 8. Therefore, release currents of 1.4 to 2 pA are too small to account for the larger sparks observed in cut or permeabilized fibers, and in cardiac myocytes. Such currents, however, may be sufficient to simulate events recorded in intact skeletal muscle fibers (16).

The discrepancy in spatial width is troubling from the standpoint of mechanism, because there is no clear way in which to modify the simulation models in order to increase spatial width to this extent. An interesting suggestion of Izu *et al.* (25) is that sparks of large width could be *platykurtic* (flat-topped), reflecting local saturation of the dye. Few truly flat-topped sparks have been reported, and they were elongated, rather than circular, suggesting cotemporal opening of many channels (37). Local saturation of the dye requires (in simulations) currents of the order of 20 pA. The existence of platykurtic sparks would therefore add to the evidence for involvement of multiple channels in spark generation.

5.2. Calculations of release flux.

An algorithm that starts from the measured fluorescence to first calculate the Ca^{2+} transient and then derive release flux was introduced by Blatter *et al.* (35) and then developed further by Lukyanenko *et al.* (36) and Ríos *et al.* (13). A simplified account is given here, following largely the latest of these references.

The first step in the procedure is deblurring. This procedure, which is quite standard, should take into account the characteristics of the specific setup, contained in its point spread function. In all confocal microscopes the *z* or vertical spread is greater (its measure σ_Z varying between 0.7 and 1.4 ìm), while the spread in the image plane (*x*-*y*) is isotropic, of the order of the wavelength of emitted light. Deblurring results in a substantial sharpening of the signal and an increase in relative amplitude (by a factor of ~ 2; ref 13).

Starting from the deblurred line scan signal $F(x,t)$, [*dye*:Ca^{2+}] (x,t) is derived as

$$[dye{:}Ca^{2+}](x,t) = dye_T(x)\,(F(x,t)-F_{min}(x))/(F_{max}(x)-F_{min}(x)). \quad (2b)$$

Then [Ca^{2+}](x,t) is obtained numerically, solving the diffusion-reaction equation that governs the evolution of [*dye*:Ca^{2+}] in time and space:

$$\frac{\partial [dye{:}Ca^{2+}](x,t)}{\partial t} = [dye](x,t)\,[Ca^{2+}](x,t)\,k^+ - [dye{:}Ca^{2+}](x,t)\,k^- + D_{dyeCa}\,\Delta[dye{:}Ca^{2+}](x,t) \quad (3)$$

where k^+ and k^- are the rate constants of the fluo-3:Ca^{2+} reaction, D_{dyeCa} is the diffusion coefficient and Ä is the laplacian operator ($\partial^2/\partial x^2 + \partial^2/\partial y^2 + \partial^2/\partial z^2$), which for all Ca^{2+} complexes is less than zero near a Ca^{2+} source. The line scan only provides the partial derivative in the *x* direction. M. Cannell (Univ. New Zealand) suggested assuming that the fluorescence increase is spherically symmetric, a function of time and the distance ($\tilde{n}$) to its center. In that case the dependence of *F* with *x* gives all the information needed to calculate the laplacian correctly, as $\partial^2/\partial x^2 + 2\,(\partial/\partial x)/x$. Once the laplacian is substituted, eqn. 3 can be solved for [Ca^{2+}], which turns out to be a sum of terms in [dye:Ca^{2+}] and its partial derivatives. Of course, this approach will give wrong results when the source (or the spark evolution) is not spherically symmetric.

Release flux is calculated from [Ca^{2+}](x,t) using a generalization of eqn. 2. The starting point is an equation, analogous to (3), that describes the evolution of free [Ca^{2+}]

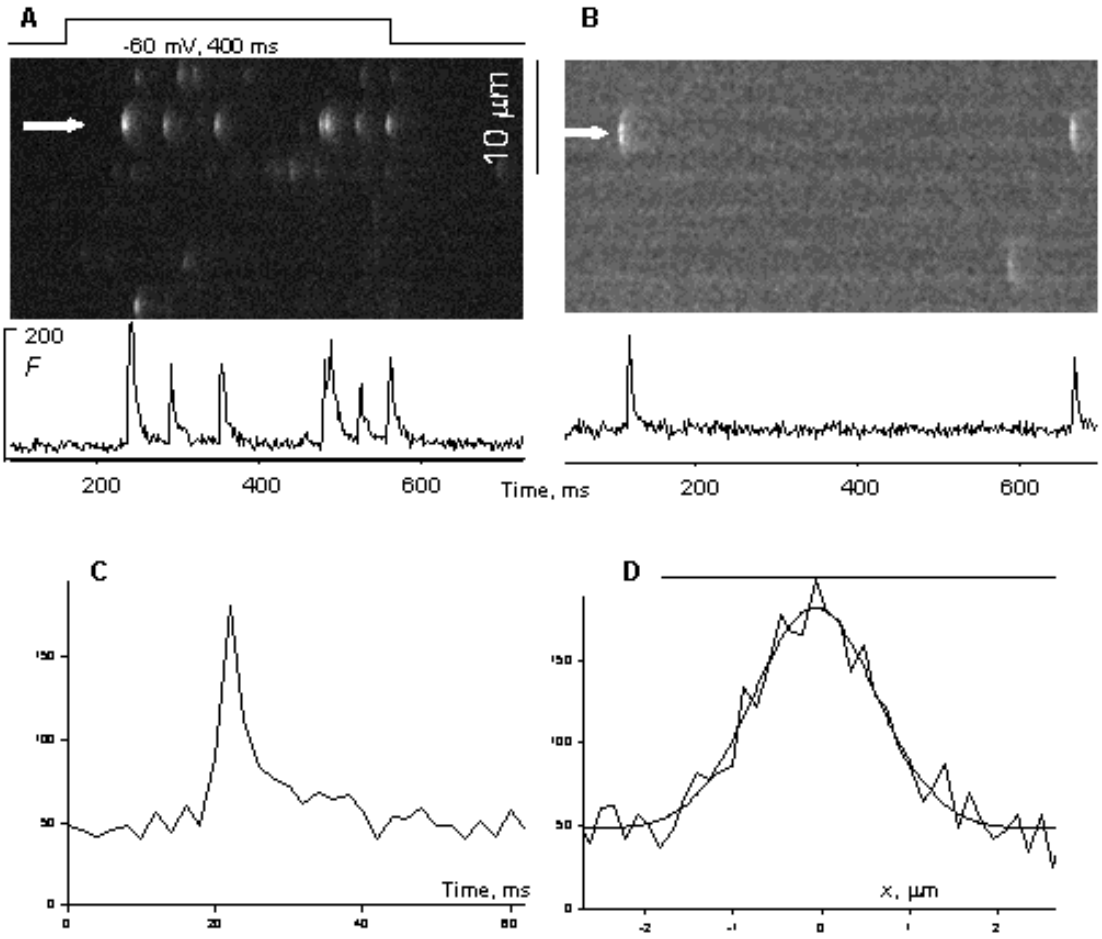

Figure 3. Morphology of large sparks. A, part of line scan image of a voltage clamped frog fiber, held at -90 mV and pulsed as shown. B, part of line scan image of a frog fiber permeabilized by saponin and immersed in a fluo 3-containing internal solution. In A and B the trace depicts fluorescence, averaged over three pixels centered at the arrow. Bar: 10ìm. C, temporal profile of the large spark in B. D, spatial profile at the maximum and best fit gaussian (of standard deviation 0.696 ìm, corresponding to a FWHM of 1.64 ìm). Methods and solutions used in A given by Shirokova *et al.* 1997. In B, total fluo 3 was 200 ìM. The images in panels A and B were obtained with similar settings, but the excitation light in A was 3 fold more intense. In B a myoplasmic dye concentration of 369 ìM was estimated, as that needed to produce the resting [dye:Ca^{2+}] (35.9 ìM, derived from F_0 and calibrations in solution), assuming [Ca^{2+}] = 100 nM and K_D = 1.03 ìM for the dye reaction (24). This large spark requires a Ca^{2+} release current of about 8 pA to account just for the Ca^{2+} bound to the dye.

$$\partial[Ca^{2+}](x,t)/\partial t = D_{Ca}\nabla[Ca^{2+}](x,t) + \mathcal{U} - \partial rem/\partial t \quad (4)$$

D_{Ca} is the diffusion coefficient of Ca^{2+}. The equation recognizes the existence of a source, of flux $\mathcal{U}$, a function of time and the spatial coordinate, and a removal system.

Hence

$$\mathcal{U} = \partial[Ca^{2+}]/\partial t - D_{Ca}\nabla[Ca^{2+}] + \partial rem/\partial t \quad (5)$$

where $\partial rem/\partial t$ is the sum of the removal terms.

This is similar to the "global" eqn. 2. It includes all its terms plus the diffusion term $-D_{Ca}\nabla[Ca^{2+}]$. Even the dimensions, concentration over time, are the same as in the global equation.

5.2.1. The removal terms

$\partial rem/\partial t$ is a sum of contributions for each buffer in the cell (the dye, parvalbumin, ATP, and sites in troponin and SR pump). An equation of the same form as 3 applied to each buffer *b*, yields the respective contribution as

$$\partial[b:Ca^{2+}]/\partial t - D_{b:Ca}\nabla[b:Ca^{2+}] \quad (6)$$

An additional term (a positive function of time, constant in space) represents SR transport.

Because the medium is assumed spatially homogeneous, the sole difference with the global eqn. 2 is the appearance of diffusion terms, one for Ca^{2+}, and one for each of the Ca^{2+} complexes with diffusible buffers. Because the sign

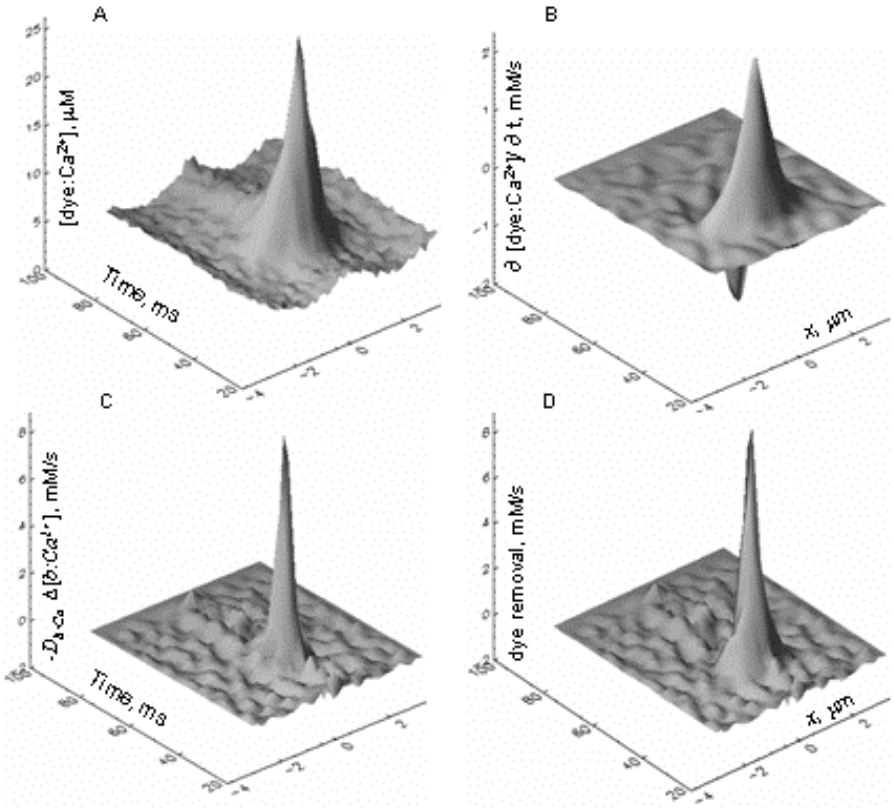

Figure 4. Dye-related removal flux. A, local distribution of [*dye*:Ca^{2+}], derived using eqn. 2b from the fluorescence average of 67 sparks elicited by depolarization (to -50 mV) in a frog fiber. The sparks were further selected for having rise times between 5 and 7 ms, and averaged by placing them centered at their peak amplitude. B, time derivative of [*dye*:Ca^{2+}]. According to eqn. 3 this rate of change results from reaction (with Ca^{2+}) and diffusion. C, the diffusion term - $D_{dye:Ca}$ Ä [*dye*:Ca^{2+}]. D, total removal flux into the dye (given by the sum of components in panels B and C, eqn. 6). The calculations in figs. 4 through 8 used parameter values listed in table 2. The fiber was prepared as described in ref. 14, in an internal reference solution containing 50 ìM fluo-3 and 5 mM ATP and 1 mM EGTA as main Ca^{2+} ligands.

of the laplacian corresponds to the curvature of the local concentration, the diffusion terms (eqn. 6) will be positive near the source (where the distribution of the Ca^{2+}-bound species can be viewed as convex, of negative curvature) and become negative at a certain distance. All contributions of course cancel, except at the source. Therefore, the calculation should give an isolated peak in a very restricted region of space.

5.2.2. Graphic example

Figures 4 to 9 illustrate the steps of the calculation and relative magnitudes of the various contributions to removal. To improve the signal to noise ratio, we start from an average of 67 sparks, which were identified automatically in several images from the same experiment. The average fluorescence, F (x, t), is deblurred and normalized dividing F by F_0, a function of x found by averaging F over time in the line scans recorded prior to the pulse.

Figure 4A shows the local concentration of the dye:Ca^{2+} complex, which in the case of fluo-3 is essentially proportional to the fluorescence. Panel B is its derivative with respect to time, which plays an important role in the calculation, not just because it participates in the calculation of free [Ca^{2+}] (eqn. 3), but also because it constitutes directly a component of removal of Ca^{2+}, in fact the only one that can be calculated with little error, giving rise to a lower bound to release flux that will be discussed later.

The dye provides an example of the contributions to Ca^{2+} removal made by all other diffusible buffers. As seen in the general equation 6 for every buffer the contribution to removal may be viewed as sum of a local rate of change, represented for the dye in panel 4B, and the diffusional term, represented in panel 4C. Like other diffusional terms, it is much narrower and large at its center than the other component. 4D shows the sum of both components of removal by the dye.

From the [dye:Ca^{2+}] (x,t), the Ca^{2+} transient is calculated by eqn. 3. It is shown in Figure 5. It is surprising that [Ca^{2+}] only reaches values of 7 ìM (up to 25

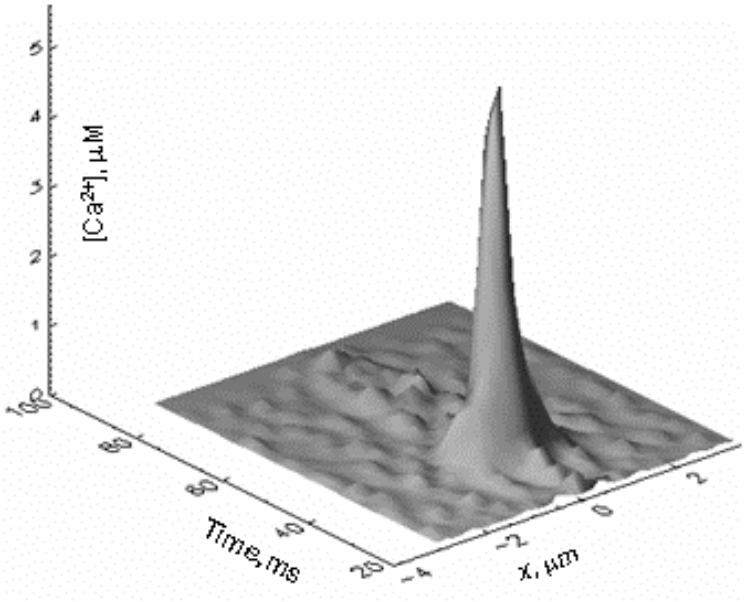

Figure 5. The Ca^{2+} transient associated to a spark. $[Ca^{2+}](x,t)$ derived from the $[dye{:}Ca^{2+}](x,t)$ of the previous figure solving eqn. 3.

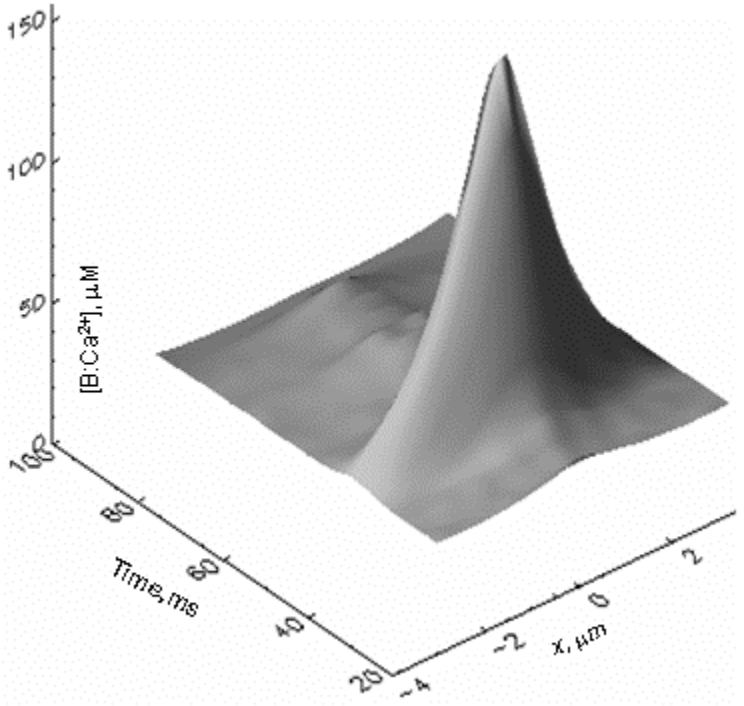

Figure 6. Ca^{2+} bound to fixed buffers. Distribution of Ca^{2+} bound to sites on troponin C and the SR pump. The calculation used the Ca^{2+} transient of Figure 5 to drive binding reactions to the sites, assumed to be homogeneously distributed, with concentrations and reaction rate constants given in table 2.

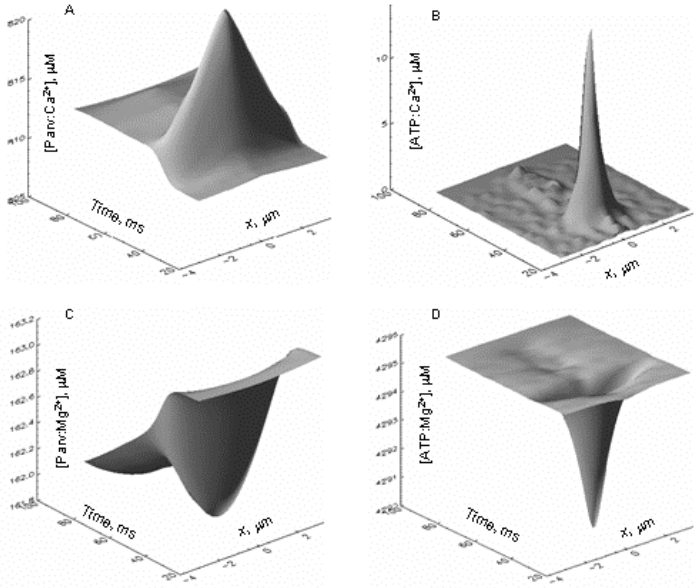

Figure 7. Removal sites shared with Mg^{2+}. A, B, distribution of Ca^{2+} bound to sites on parvalbumin and ATP. C, D, distribution of the Mg^{2+}-bound forms of the same ligands. Note that in the present example, with Mg^{2+} present at a low concentration of 0.61 mM, over 80% of ATP and ~ 16% of parvalbumin are bound to Mg^{2+}. At greater, presumably more physiological [Mg^{2+}], the attenuating effect of this ion on Ca^{2+} removal

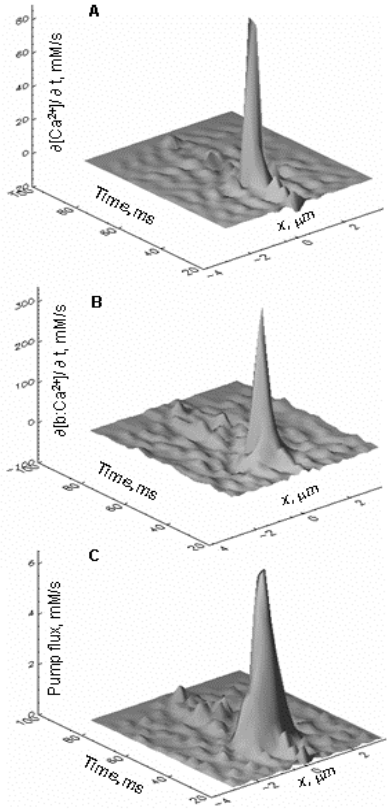

Figure 8. Three main terms of release flux. A, diffusional free Ca^{2+} term: $-D_{Ca}$ Ä[Ca^{2+}]. B, removal flux by ligands other than the dye. C, flux of transport by the SR pump, calculated as proportional to the square of the occupancy of its binding sites.

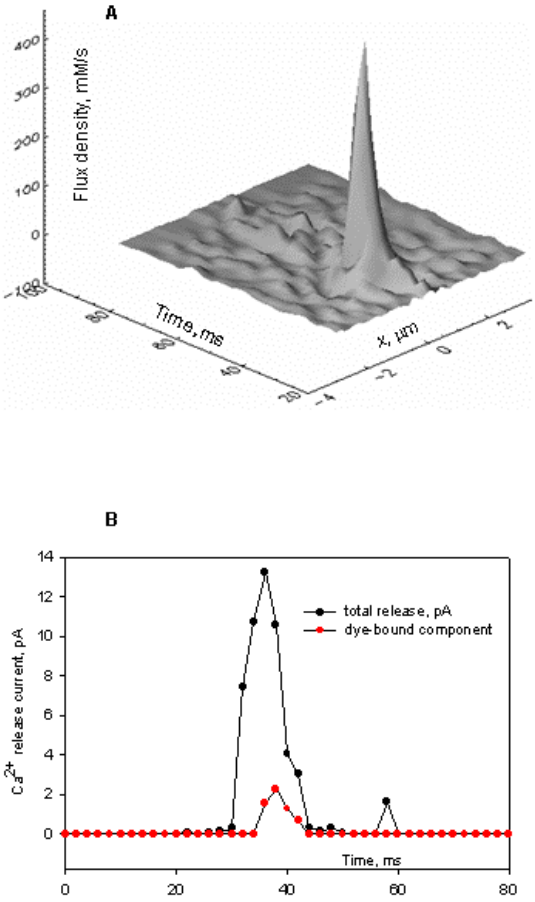

Figure 9. Ca^{2+} release flux. A, release flux calculated as sum of all terms in Figure 8 plus the dye removal term in Figure 4D. B, the Ca^{2+} release current, calculated from the volume integral of the flux in A. The current in red is calculated from the integral of the dye removal term.

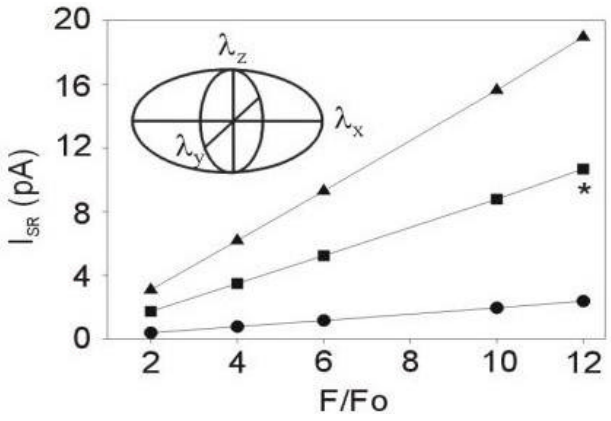

Figure 10. Lower bounds of Ca^{2+} release current. For these calculations, the fluorescent indicator is the only buffer. Spark dimensions are given by the FWHM (in ìm) along the x, y, and z axes, (ëx, ëy, ëz). The inset shows a schematic of an ellipsoidal spark. For a spherical spark ëx = ëy = ë z. Circles show the current required to produce a spherical spark whose FWHM is 1 ìm; squares are for an elliptical spark (of dimensions 2, 1.5, 1.5) and triangles are for a spherical spark (2, 2, 2) . The current varies linearly with the spark amplitude F/F0, and the slopes are proportional to the spark volume. Note that this lower estimate is consistent with that represented by the red trace in Figure 9B, considering that the spark analyzed in that figure had a FWHM of 1.5 ìm and amplitude ~2. Reproduced from Izu *et al*. (25).

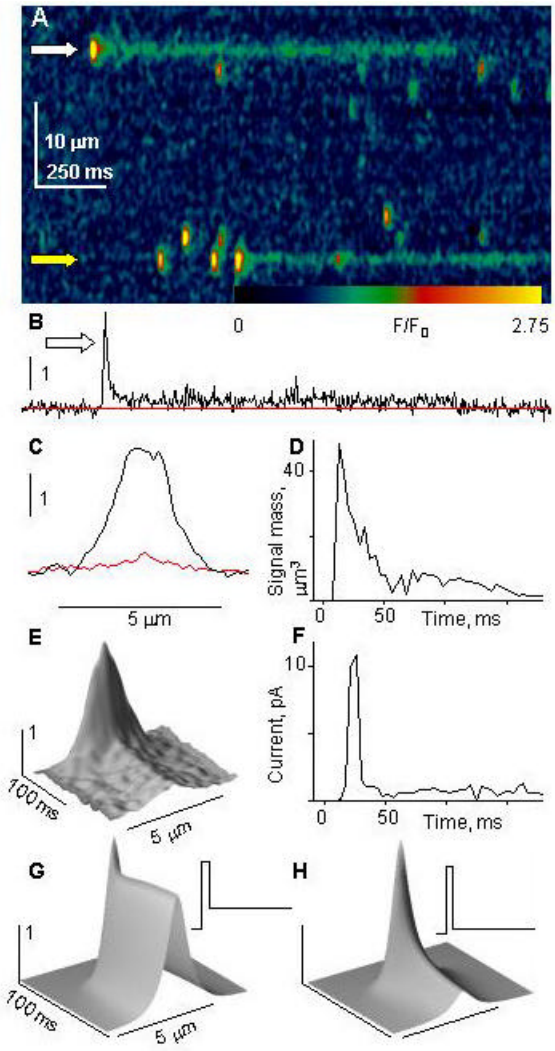

Figure 11. Release flux in drug-induced channel openings. A, image of a permeabilized cell, immersed in solution with 100 nM imperatoxin A. B, temporal profile of F/F_0 at white arrow. C, spatial profile of F/F_0 at the peak of the starter event and its average (red) during the long event that follows. D, time course of signal mass. E, F/F_0 in an average of 9 long events selected by their large amplitude. F, release current, calculated from the average event. G, simulated fluorescence event for a Ca^{2+} source of initial current 10 pA, lasting 6 ms, followed by a steady current of 3.3 pA (inset). H, simulation where the opening at 10 pA is followed by a steady 0.5 pA current. The source diameter was 0,05 ìm. Details and parameter values of the simulation described in Ríos *et al.* (13). Figure reprinted from González *et al.* (31).

ìM for the largest sparks). In simulations, the concentration near the channel mouth may reach hundreds of ìM. Comparable values are not reached here largely because of the coarse Agrain@, 145 nm per pixel in the present calculation. In trials with greater spatial resolution much greater central values were found. The values of release flux density also increased, but only in a small volume, and the calculated current did not change significantly.

The rest is a repeated calculation of removal terms, given by eqn. 6. These are formally similar to the ones shown for the dye. Figure 6 illustrates the sum of the concentrations of Ca^{2+} bound to fixed removal molecules, in this case, sites of the SR pump and troponin C. Removal by these elements is simply the rate of change of the concentration shown.

The evolutions in space and time of [Parvalbumin:Ca^{2+}] and [ATP:Ca^{2+}] are in Figure 7. In both cases Mg^{2+} competes for the binding sites. The corresponding Mg^{2+} complexes are also shown. The local parvalbumin contribution to removal is small, in part because of the occupancy by Mg^{2+}. ATP instead makes a sizable local contribution, due to its high reaction speed and concentration. The experimental sparks in these

calculations were obtained at a relatively low [Mg^{2+}] (610 ìM). At higher, presumably more physiological [Mg^{2+}], the attenuating effect of this ion on removal will be greater.

Figure 8 compares three main terms of release flux. The first term in eqn. 5, rate of change in [Ca^{2+}], is negligible. In A is the diffusional free Ca^{2+} term, which is relatively large due to the very sharp local [Ca^{2+}] gradient. In B is the removal flux by ligands other than the dye. The dominant component of this term in the example is removal by ATP. In C is the flux of transport by the SR pump, calculated as proportional to the square of the occupancy of its binding sites. It is comparatively very small, which explains why simulations assuming a homogeneous cytoplasm yield results very similar to those that try to reproduce the spatial location of troponin and the SR pump (27, 33). In Figure 9A is total release flux, from which the release Ca^{2+} current, plotted in B, is calculated by integration over the volume of the source. As shown in 9 B, the release current reached ~14 pA in the example. In calculations using large sparks we have found values close to 20 pA (13).

5.2.3. A lower bound

As discussed above, the calculation involves terms corresponding to different ligands, of which one must assume concentration, diffusion coefficient (of both free and Ca^{2+}-bound forms) and reaction rate constants. The exception is the dye, for which the total concentration may be measured, and the concentration of the Ca^{2+}-bound form directly derived from the fluorescence. Thus the dye removal contribution, illustrated in Figure 4D, is the only one that can be calculated with reasonable certainty, and constitutes a robust lower bound in the calculation of release flux. The current of removal by the dye (plotted in red in Figure 9B) is calculated as volume integral of the flux. In the example, where the total dye concentration was 50 ìM, it constitutes a minor component. When the dye concentration is greater, the contribution grows accordingly. In conditions of high [dye], Ríos *et al.* (13) calculated a value of 8 pA for this lower bound, using large sparks in experiments on permeabilized fibers (see example in Figure 3).

5.3. Other estimates of release current.

Other estimates have been reported, but for sparks of cardiac muscle. Using essentially the same analysis described above, Blatter *et al.* (35) found a value of 3 pA for cat atrial cells. The reason for the lower value is that the amplitude of the sparks was lower, and also the removal model used to describe the atrial cytoplasm implied a lower buffer/removal capacity than in the skeletal muscle study. Lukyanenko *et al.* (36), who applied a similar technique to rat ventricular myocytes, did not report integrated release current but obtained values of release flux 2 to 10 times lower than Blatter *et al.* (35). Again, the explanation for the difference resides mainly in the smaller size of the sparks studied.

It is possible that the underlying release in cardiac sparks is smaller than in skeletal muscle: Wang *et al.* (44) recorded simultaneously sparks and Asparklets@ due to opening of single L-type Ca^{2+} channels in the same dyadic unit of ventricular myocytes. The separate measurement of current underlying sparklets provided an accurate calibration of the optical signals, yielding a current of 2.1 pA for the spark. Again, sparks were of small size, hence the result is not in conflict with any of the other estimates.

Izu and colleagues (25) took an approach similar to the Alower bound@ above Bthat is, no buffers, other than 50 ìM dye. They calculated a minimum current needed to account for a spark of given amplitude and width, assumed to be a Gaussian function in space. Their results are represented in fig.10, as a function of spark amplitude, for three different assumptions regarding spatial width. In agreement with our example above, their minimum current for a spark of amplitude 2 and width 1.5 ìm would be nearly 2 pA. These authors also presented sparks of much greater amplitude and width, and concluded that a current of ~20 pA underlies sparks. The events studied by Izu *et al.* (25) were greater than in the previous studies with cardiac muscle. They were similar to those studied by Ríos *et al.* (13) in skeletal muscle, and so were their estimates of current.

There is therefore general agreement regarding the derivation of release current. The disagreements that remain are due to the divergence in spark sizes recorded in different laboratories. Because sparks as objects have variable amplitude, the associated release current will surely be variable. It is also worth recalling the 3rd order relationship between spatial width and signal mass. Thus the narrow events reported by Baylor *et al.* (16) in intact frog fibers should result from a much lower release current than the examples given above.

5.4. Artificially induced events

Finally, we will show how the calculations of release flux can be applied to events other than sparks. In the example shown in fig.11 (31), events were induced by application of imperatoxin A, extracted from scorpion venom. The drug induces the long-lasting events of low amplitude marked by arrows in panel A. These events (described in detail in ref. 45) correspond to long lasting open states of reduced conductance, induced by the drug in bilayer experiments (46, 47). As shown, they usually start with a spark-like event of greater underlying current. In B and C are temporal and spatial profiles of the event indicated with a white arrow in A. In D is its signal mass, which decays from an early peak to a sustained level, about 8-fold lower. To evaluate the underlying current, the release calculation algorithm described above was applied to an average of 9 such events, represented in E. The resulting release current (panel F) peaks at 11.3 pA and then decays to a steady value averaging 0.68 pA. The peak/steady ratio is 16.6.

A recent report (17) shows that sparks of mammalian skeletal muscle often end with a prolonged Atail@ of lower intensity. By analogy with an earlier observation of González *et al.* (14) on averages of sparks

Table 2. Values of parameters used by the release flux algorithm. Parv, parvalbumin. Trop, troponin. [Ca^{2+}] was 0.1 ìM. [Mg^{2+}] was 0.61 mM.

Parameter	Value	Ref
Fluo-3:Ca ON-rate	3.2 10^7 $M^{-1}s^{-1}$	24
Fluo-3 dissoc. const.	1.03 µM	24
EGTA:Ca ON-rate	0.2 10^7 $M^{-1}s^{-1}$	39
EGTA dissoc. Const	1 µM	39
Trop:Ca ON-rate	5.7 10^6 $M^{-1}s^{-1}$	6
Trop:Ca OFF-rate	11.4 s^{-1}	6
ATP:Ca ON-rate	1.5 10^8 $M^{-1}s^{-1}$	40
ATP:Ca OFF-rate	3 10^4 s^{-1}	40
ATP:Mg ON-rate	1.5 10^6 $M^{-1}s^{-1}$	40
ATP:Mg OFF-rate	195 s^{-1}	40
Parv:Ca ON-rate	1.25 10^8 $M^{-1}s^{-1}$	6
Parv:Ca OFF-rate	0.5 s^{-1}	6
Parv:Mg ON-rate	3.3 10^4 $M^{-1}s^{-1}$	6
Parv:Mg OFF-rate	3 s^{-1}	6
Maximum pump rate	9.8 mM s^{-1}	†
[Parvalbumin]	1 mM	6
[Pump sites]	0.2 mM	6
[EGTA]	1 mM	*
[ATP]	5 mM	*
D_{Ca}	3.5 10^{-6} cm^2s^{-1}	41
D_{dye}	2 10^{-7} cm^2s^{-1}	24
D_{ATP}	1.4 10^{-6} cm^2s^{-1}	40
D_{parv}	2.6 10^{-7} cm^2s^{-1}	42
D_{EGTA}	3.6 10^{-7} cm^2s^{-1}	43

* value in solution, H a value that fits global Ca^{2+} transients when other parameters of removal had the values listed

from amphibian muscle under voltage clamp, they termed these prolongations Aembers@. The analogy with the events induced by imperatoxin A indicates that the release flux associated with embers is much lower than that during the initial spark.

5.5. Non-events

A final question, indicated in the Introduction, is whether sparks constitute all of Ca^{2+} release, or there is a different form. Shirokova and Rios (48) showed that the presence of the local anesthetic tetracaine results in release without sparks in cells that normally have them. In these experiments, a faint Anon-event@ increase in fluorescence appeared upon very low depolarization in the absence of the drug, suggesting that this form of release exists normally, and that it is uncovered rather than induced by the drug. Release flux in such cases should be extremely low, and clearly different in temporal and spatial properties from that in sparks. This release has been compared with the so-called Acalcium quarks@, postulated to be manifestations of single channel activity (Egger and Niggli, this volume). One possibility is that it courses through channels directly controlled by voltage sensors in the T membrane. Such activity might produce the embers that follow or sometimes precede sparks (section 5.4), or diffuse release in conditions that inhibit spark production.

6. CONSEQUENCES AND CONCLUSIONS

6.1. Single channels and sparks

The current underlying a spark, 1.5 to 20 pA, should be compared with the physiological unitary current. Mejía-Alvarez *et al.* (49) reported a unitary current of 0.35 to 0.5 pA through dog cardiac channels in bilayers, carrying Ca^{2+} under [Ca^{2+}] gradients of physiological magnitude and direction. Kettlun *et al.* (50) reported a unitary current of ~ 0.7 pA in Ca^{2+} release channels from frog skeletal muscle. The reason for the greater current was in part that the channels were kept open by 10 mM caffeine (to avoid underestimates due to flickering). Under the same conditions the cardiac channels carried a current of ~0.5 pA. Hence a current of 2.1 pA, as reported by Wang *et al.* (44), would require 4 simultaneously open channels. A much greater number of open channels would be required with the estimates of spark current of Izu *et al.* (25). For skeletal muscle sparks, the number of open channels would have to be 10 to 30. A somewhat lower number is obtained from the analysis of release current associated to the events induced by imperatoxin A.

The idea that sparks are produced by several channels is consistent with evidence of multifocal origin of sparks in cardiac muscle (51, 35), and with the demonstration (37) of sources of spatially resolved size, extending along the Z lines in skeletal muscle. It is quite inconsistent with the demonstration (32) that the rising phase of sparks both starts and ends abruptly, as if a single channel gated open and close. According to reference 32, if many channels contributed, they should open and close in unison.

6.2. Single channels and global release flux

These estimates of current per channel or per spark are roughly consistent with whole cell estimates of release flux. We update here a calculation of Shirokova *et al.* (18). The maxima of flux density under voltage clamp are near 180 mM/s in the frog (2,52). The density of release channels can be calculated from morphometry or from ryanodine binding measurements. The ratio of T tubule length to fiber volume is 0.82 $ìm^{-2}$ in frog twitch muscle (53). Assuming that 70% of this length is junctional and contains a double row of release channels at 30 nm spacing on each side, the number of channels per liter is 0.7 H33 channels/row/ìm H2 rows/junction H2 junctions/triad H0.82 $ìm^{-2}$, or 1.08H10^{17} channels per liter of the aqueous myoplasmic volume. At 100% activation, such channels passing 0.7 pA would generate a flux density of 360 mM/s. Using the unitary current figure of Kettlun *et al.* (50), the largest release would require opening of 50% of the channels.

It is relevant in this regard that the ratio of ryanodine to dihydropyridine sites expected from the structural alignment model of Block *et al.* (54) is 0.5, a value that is found approximately in isolated membrane fractions of rabbit or human muscle (55, 56, 57). In frog muscle the value is instead about 1.5 (56, 57), which would suggest an excess of release channels, probably outside the double row. This would predict an even larger maximum release in the morphometric-based calculation above, again indicating that the estimates of release per channel and release per spark are consistent with the greatest estimates of global release, requiring even in those cases values of open probability well under unity.

In summary, estimates of Ca^{2+} release current underlying sparks range between 1.4 and 30 pA, perhaps somewhat greater in skeletal than in cardiac muscle. At their low end, the estimates are consistent with generation of sparks by one or two channels, but the results are easier to explain if several channels, from as little as four to as many as 60, cooperate in their generation (and in some cases gate essentially in unison). Both the release flux and the open time may vary among individual sparks, leading to their varied size and shape. In sparks that end with an ember, release flux must fall from an early level consistent with many open channels, to a level requiring the current of one or two channels. The continued examination of Ca^{2+} release flux appears to be an essential requisite for the interpretation of sparks and their place in calcium signaling.

7. ACKNOWLEDGMENTS

We are grateful to all the colleagues and collaborators who allowed us to reprint figures from their work. We were supported by the National Institutes of Health (NIH) and Conicyt, Uruguay.

8. REFERENCE

1. Cheng H, W. J. Lederer & M .B. Cannell: Calcium sparks: elementary events underlying excitation-contraction coupling in heart muscle. *Science* 262, 740-744 (1993)

2. Shirokova N, J. García, G. Pizarro & E. Ríos: Ca^{2+} release from the sarcoplasmic reticulum compared in amphibian and mammalian skeletal muscle. *J Gen Physiol* 107, 1-18 (1996)

3. Melzer W, E. Ríos & M. F. Schneider: Time course of calcium release and removal in skeletal muscle fibers. *Biophys J* 45, 637-641 (1984)

4. Melzer W, E. Ríos & M. F. Schneider: A general procedure for determining the rate of calcium release from the sarcoplasmic reticulum in skeletal muscle fibers. *Biophys J* 51, 849-863 (1987)

5. Ríos E. & G. Pizarro: Voltage sensors and channels of excitation-contraction coupling. *News Physiol Sci* 3, 223-227 (1988)

6. Baylor S. M, W. K. Chandler & M. W. Marshall: Sarcoplasmic reticulum calcium release in frog skeletal muscle fibres estimated from Arsenazo III calcium transients. *J Physiol (Lond)* 344, 625-666 (1983)

7. Ríos E. & G. Pizarro: Voltage sensor of excitation-contraction coupling in skeletal muscle. *Physiol Rev* 71, 849-908 (1991)

8. González A. & E. Ríos: Perchlorate enhances transmission in skeletal muscle excitation-contraction coupling. *J Gen Physiol* 102, 373-421 (1993)

9. Pape P. C, D. S. Jong & W. K. Chandler: Calcium release and its voltage dependence in frog cut muscle fibers equilibrated with 20 mM EGTA. *J Gen Physiol* 106, 259-336 (1995)

10. Rakowski R. F, P. M. Best & M. R. James-Kracke: Voltage dependence of membrane charge movement and calcium release in frog skeletal muscle fibres. *J Muscle Res Cell Motil* 6, 403-433 (1985)

11. García J, G. Pizarro, E. Ríos & E. Stefani: Effect of the calcium buffer EGTA on the "hump" component of charge movement in skeletal muscle. *J Gen Physiol* 97, 885-896 (1991)

12. Baylor S. M. & S. Hollingworth: Measurement and Interpretation of Cytoplasmic [Ca^{2+}]. *News Physiol Sci* 15, 19-26 (2000)

13. Ríos E, M. D. Stern, A. González, G. Pizarro &, N. Shirokova: Calcium release flux underlying Ca^{2+} sparks of frog skeletal muscle. *J Gen Physiol* 114, 31-48 (1999)

14. González A, W. G. Kirsch, N. Shirokova, G. Pizarro, M. D. Stern & E. Ríos: The spark and its ember: separately gated local components of Ca^{2+} release in skeletal muscle. *J Gen Physiol* 115, 139-158 (2000a)

15. Lacampagne A, M. G. Klein & M. F. Schneider: Modulation of the frequency of spontaneous sarcoplasmic reticulum Ca^{2+} release events Ca^{2+} sparks by myoplasmic [Mg^{2+}] in frog skeletal muscle. *J Gen Physiol* 111, 207-224 (1998)

16. Baylor S. M, J. Peet, W. K. Chandler & S. Hollingworth: Comparison of resting and voltage activated calcium sparks in intact skeletal muscle fibers of R. *Temporaria* and *R. Pipiens. Biophys J* 80, 66a (2001)

17. Kirsch W, D. Uttenweiler & R. H. A. Fink: Spark- and ember-like elementary Ca^{2+} release events in skinned fibres of adult mammalian skeletal muscle. *J Physiol* in press (2001)

18. Shirokova N, A. Gonzalez, W. G. Kirsch, E. Rios, G. Pizarro, M. D. Stern & H. Cheng: Calcium sparks: release packets of uncertain origin and fundamental role. *J Gen Physiol* 113, 377-384 (1999)

19. Tanaka H, K. Nishimaru, T. Sekine, T. Kawanishi, R Nakamura, K. Yamagaki & K. Shigenobu: Two-dimensional millisecond analysis of intracellular Ca^{2+} sparks in cardiac myocytes by rapid scanning confocal microscopy: increase in amplitude by isoproterenol. *Biochem Biophys Res Commun* 233, 413-418 (1997)

20. Lukyanenko V. & S. Györke: Ca^{2+} sparks and Ca^{2+} waves in saponin-permeabilized rat ventricular myocytes. *J Physiol* 521, 575-585 (1999)

21. Smith G. D, J. E. Keizer, J. D. Stern, W. J. Lederer & H. Cheng: A simple numerical model of calcium spark formation and detection in cardiac myocytes. *Biophys J* 75, 15-32 (1998)

22. Santana L. F, E. G. Kranias & W. J. Lederer: Calcium sparks and excitation-contraction coupling in phospholamban-deficient mouse ventricular myocytes. *J Physiol* 503, 21-29 (1997)

23. Wier W. G, H. E. ter Keurs, E. Marban , W. D. Gao & C. W. Balke: Ca^{2+} 'sparks' and waves in intact ventricular muscle resolved by confocal imaging. *Circ Res* 81, 462-469 (1997)

24. Harkins A. B, N. Kurebayashi & S. M. Baylor: Resting myoplasmic free calcium in frog skeletal muscle fibers estimated with fluo-3. *Biophys J* 65, 865-881 (1993)

25. Izu L. T, J. R. Mauban, C. W. Balke, W. G. Wier: Large currents generate cardiac Ca^{2+} sparks. *Biophys J* 80, 88-102 (2001)

26. González A, J. Zhou, W. G. Kirsch, D. Uttenweiler, R. A. Fink, E. Ríos & G. Brum: Morphology of Ca^{2+} sparks of mammalian muscle. *Biophys J* Abst in press (2002)

27. Pratusevich V. R. & C. W. Balke: Factors shaping the confocal image of the calcium spark in cardiac muscle cells. *Biophys J* 71, 2942-2957 (1996)

28. Cheng H, L. S. Song, N. Shirokova, A. González, E. G. Lakatta, E. Ríos & M. D. Stern: Amplitude distribution of calcium sparks in confocal Images. Theory and studies with an automatic detection method. *Biophys J* 76, 606-617 (1999)

29. Izu L. T, W. G. Wier & C. W. Balke: Theoretical analysis of the Ca^{2+} spark amplitude distribution. *Biophys J* 75, 1144-1162 (1998)

30. Ríos E, N. Shirokova, W. Kirsch, G. Pizarro, M. D. Stern, H. Cheng & A. González: A preferred amplitude of calcium sparks in skeletal muscle. *Biophys J* 80, 169-183 (2001)

31. González A, W. G. Kirsch, N. Shirokova, G. Pizarro, G. Brum, I. N. Pessah, M. D. Stern, H. Cheng & E. Ríos: Involvement of multiple intracellular release channels in calcium sparks of skeletal muscle. *Proc Natl Acad Sci USA* 97, 4380-4385 (2000)

32. Lacampagne A, C. W. Ward, M. G. Klein & M. F. Schneider: Time course of individual voltage-activated Ca^{2+} sparks recorded at ultra-high time resolution in frog skeletal muscle. *J Gen Physiol* 113, 187-198 (1999)

33. Jiang Y. H, M. G. Klein & M. F. Schneider: Numerical simulation of Ca^{2+} "sparks" in skeletal muscle. *Biophys J* 77, 2333-2357 (1999)

34. Sun X. P, N. Callamaras, J. S. Marchant & I. Parker: A continuum of InsP3-mediated elementary Ca^{2+} signalling events in Xenopus oocytes. *J Physiol* 509, 67-80 (1998)

35. Blatter L. A, J. Hüser & E. Ríos: Sarcoplasmic reticulum Ca^{2+} release flux underlying Ca^{2+} sparks in cardiac muscle. *Proc Natl Acad Sci USA* 94, 4176-4181 (1997)

36. Lukyanenko V, T. F. Wiesner & S. Gyöke. Termination of Ca^{2+} release during Ca^{2+} sparks in rat ventricular myocytes. *J Physiol* 507, 667-677 (1998)

37. Brum G, A. González, J. Rengifo, N. Shirokova & E. Ríos: Fast imaging in two dimensions resolves extensive sources of Ca^{2+} sparks in frog skeletal muscle. *J Physiol* 528, 419-433 (2000)

38. Ríos E. & M. D. Stern:. Calcium in close quarters: microdomain feedback in excitation-contraction coupling and other cell biological phenomena. *Annu Rev Biophys Biomol Struct* 26, 47-82 (1997)

39. Smith P. D, G. W. Liesegang, R. L. Berger, G. Czerlinski & R. J Podolsky: A stopped-flow investigation of calcium ion binding by ethylene glycol bis(beta-aminoethyl ether) -N,N'-tetraacetic acid. *Anal Biochem* 143, 188-195 (1984)

40. Baylor S. M. & S. Hollingworth: The transient binding of calcium to ATP and diffusion of Ca-ATP help shape the amplitude and time course of the myoplasmic free Ca transients. *Biophys J* 74, 235a (1998)

41. Kushmerick M. J. & R. J. Podolsky: Ionic mobility in muscle cells. *Science* 166, 1297-1298 (1969)

42. Pechère J. F, J. P. Capony & J. Demaille: Evolutionary aspects of the structure of muscular parvalbumins. *Syst Zool* 22, 533-548 (1973)

43. Pizarro G, L. Csernoch, I. Uribe, M. Rodriguez & E. Rios: The relationship between Q gamma and Ca release from the sarcoplasmic reticulum in skeletal muscle. *J Gen Physiol* 97, 913-947 (1991)

44. Wang S. Q, L. S. Song, E. G. Lakatta & H. Cheng: Ca^{2+} signalling between single L-type Ca^{2+} channels and ryanodine receptors in heart cells. *Nature* 410, 592-596 (2001)

45. Shtifman A, C. W. Ward, J. Wang, H. H. Valdivia & M. F. Schneider: Effects of imperatoxin A on local sarcoplasmic reticulum Ca^{2+} release in frog skeletal muscle. *Biophys J* 79, 814-827 (2000)

46. Tripathy A, W. Resch, L. Xu, H. H. Valdivia & G. Meissner: Imperatoxin A induces subconductance states in Ca^{2+} release channels ryanodine receptors of cardiac and skeletal muscle. *J Gen Physiol* 111, 679-690 (1998)

47. Gurrola G. B, C. Arevalo, R. Sreekumar, A. J. Lokuta, J. W. Walker & H. H. Valdivia: Activation or ryanodine receptors by imperatoxin A and a peptide segment of the II-III loop of the dihydropyridine receptor. *J Biol Chem* 274, 7879-7886 (1999)

48. Shirokova N. & E. Ríos: Small event Ca^{2+} release: a probable precursor of Ca^{2+} sparks in frog skeletal muscle. *J Physiol* 502, 3-11 (1997)

49. Mejía-Alvarez R, C. Kettlun, E. Ríos, M. D. Stern & M. Fill: Unitary Ca^{2+} current trough cardiac ryanodine receptor channels under quasi-physiological ionic conditions. *J Gen Physiol* 113, 177-186 (1999)

50. Kettlun C, A. González, W. Nonner, E. Ríos & M. Fill: Ryanodine receptor unitary Ca^{2+} current is greater in frog skeletal muscle than in mammalian heart. *Biophys J* 78, 2576 (2000)

51. Parker I, W. J. Zang & W. G. Wier: Ca^{2+} sparks involving multiple Ca^{2+} release sites along Z-lines in rat heart cells. *J Physiol* 497, 31-38 (1996)

52. Mobley B. A & B. R. Eisenberg: Sizes of components in frog skeletal muscle measured by methods of stereology. *J Gen Physiol* 66, 31-45 (1975)

53. Block B. A, T. Imagawa, K. P. Campbell & C. Franzini-Armstrong: Structural evidence for direct interaction between the molecular components of the transverse tubule/sarcoplasmic reticulum junction in skeletal muscle. *J Cell Biol* 107, 2587-2600 (1988)

54. Bers D. M. & V. M. Stiffel: Ratio of ryanodine to dihydropyridine receptors in cardiac and skeletal muscle and implications for E-C coupling. *Am J Physiol* 264, C1587-C1593 (1993)

55. Margreth A, E. Damiani & G. Tobaldin: Ratio of dihydropyridine to ryanodine receptors in mammalian and frog twitch muscles in relation to the mechanical hypothesis of excitation-contraction coupling. *Biochem Biophys Res Commun* 197, 1303-1311 (1993)

57. Anderson K, A. H. Cohn & G. Meissner: High-affinity [^{3}H]PN200-110 and [3H]ryanodine binding to rabbit and frog skeletal muscle. *Am J Physiol* 266, C462-C466 (1994)

58. Cheng H, M. R. Lederer, W. J. Lederer & M. B. Cannell: Calcium sparks and $[Ca^{2+}]_i$ waves in cardiac myocytes. *Am J Physiol Cell* 270, C148-C159 (1996)

footnotes:

[1] Unlike Baylor *et al*. (1983), Melzer and coworkers included transport by the SR pump in their removal model, hence their *R* is release proper, rather than the net balance of SR fluxes yielded by the other method.

[2] In a Gaussian approximation of sparks, the volume integral of a spherically symmetric Gaussian function of standard deviation ó and central value 1 is $(2ð)^{3/2}ó^3$ = B.

Then the signal mass of a spark of amplitude A should be AB. For Gaussian sparks, FWHM = 2 (2 ln2)$^{\mathbf{2}}$ ó; then signal mass = A (ð/4ln2)$^{3/2}$ (FWHM)^3. This is greater than the approximation of Shirokova *et al.* by a factor of 2.304.

[3] In general, flux is defined as a rate of movement of matter across the unit area of a defined surface, and it has vectorial properties. In the present analysis, there is no specified surface, hence the flux is defined as a scalar, and is distributed in the volume, thereby losing one spatial dimension.

[4] Calculation Details. The terms $[b{:}Ca^{2+}]$ are calculated from the function $[Ca^{2+}](x,t)$ solving for $[b{:}Ca^{2+}]$ the diffusion-reaction equation of form 3 for the corresponding buffer. In general this requires simultaneously solving an equation for the free buffer (see for instance eqns. 1-4 in ref 38). This is avoided assuming that the free buffer and its Ca^{2+}-complex have the same diffusion coefficient, or equivalently that total buffer concentration is constant everywhere. In the case of parvalbumin and ATP, buffers that react with both Ca^{2+} and Mg^{2+}, diffusion reaction equations of the form 3 still apply, but $[b{:}Ca^{2+}]$ is in both cases equal to $[b]_T$-$[b]$-$[b{:}Mg^{2+}]$ (where $[b]_T$ is the total concentration of buffer), and $[b{:}Mg^{2+}]$, a function of space and time, is calculated from its own diffusion-reaction equation, (7) assuming $[Mg^{2+}]$ to be constant.

Key Words: Sarcoplasmic Reticulum; Excitation-Contraction Coupling; Confocal Microscopy; Skeletal Muscle; Cardiac Muscle, Review

Send correspondence to: Dr E. Ríos, Department of Molecular Biophysics and Physiology, Rush University, 1750 W. Harrison Street, Chicago, IL 60612, Tel:312-942-2081. Fax: 312-942-8711, E-mail: erios@rush.edu